

GA-A23995

# METHANE PENETRATION IN DIII-D ELMing H-MODE PLASMAS

by

W.P. WEST, C.J. LASNIER, D.G. WHYTE, R.C. ISLER, T.E. EVANS,  
G.L. JACKSON, D.L. RUDAKOV, M.R. WADE, and J. STRACHAN

JUNE 2002

## DISCLAIMER

This report was prepared as an account of work sponsored by an agency of the United States Government. Neither the United States Government nor any agency thereof, nor any of their employees, makes any warranty, express or implied, or assumes any legal liability or responsibility for the accuracy, completeness, or usefulness of any information, apparatus, product, or process disclosed, or represents that its use would not infringe privately owned rights. Reference herein to any specific commercial product, process, or service by trade name, trademark, manufacturer, or otherwise, does not necessarily constitute or imply its endorsement, recommendation, or favoring by the United States Government or any agency thereof. The views and opinions of authors expressed herein do not necessarily state or reflect those of the United States Government or any agency thereof.

# METHANE PENETRATION IN DIII-D ELMing H-MODE PLASMAS

by

W.P. WEST, C.J. LASNIER,<sup>†</sup> D.G. WHYTE,<sup>‡</sup> R.C. ISLER,<sup>◇</sup> T.E. EVANS,  
G.L. JACKSON, D.L. RUDAKOV,<sup>‡</sup> M.R. WADE,<sup>◇</sup> and J. STRACHAN<sup>△</sup>

<sup>†</sup>Lawrence Livermore National Laboratory

<sup>†</sup>University of California, San Diego

<sup>†</sup>Oak Ridge National Laboratory

<sup>†</sup>Princeton Plasma Physics Laboratory

This is a preprint of a paper presented at the 15th International Conference on Plasma Surface Interactions in Controlled Fusion Devices, May 27-31, 2002, in Gifu, Japan, and to be published in the *Proceedings*.

Work supported by  
the U.S. Department of Energy  
under Contracts DE-AC03-99ER54463, W-7405-ENG-48,  
DE-AC05-00OR22725, DE-AC02-76CH03073 and Grant DE-FG03-95ER54294

GA PROJECT 30033  
JUNE 2002

**ABSTRACT**

Carbon penetration into the core plasma during midplane and divertor methane puffing has been measured for DIII-D ELMing H-mode plasmas. The methane puffs are adjusted to a measurable signal, but global plasma parameters are only weakly affected (line average density,  $\langle n_e \rangle$  increases by  $< 10\%$ , energy confinement time,  $\tau_E$ , drops by  $< 10\%$ ). The total carbon content is derived from  $C^{+6}$  density profiles in the core measured as a function of time using charge exchange recombination spectroscopy. The methane penetration factor is defined as the difference in the core content with the puff on and puff off, divided by the carbon confinement time and the methane puffing rate. In ELMing H-mode discharges with ion  $\nabla B$  drift direction into the X-point, increasing the line averaged density from  $5$  to  $8 \times 10^{19} \text{ m}^{-3}$  dropped the penetration factor from  $6.6\%$  to  $4.6\%$  for main chamber puffing. The penetration factor for divertor puffing was below the detection limit ( $< 1\%$ ). Changing the ion  $\nabla B$  drift direction to away from the X-point decreased the penetration factor by more than a factor of five for main chamber puffing.

## 1. EXPERIMENT

The plasma facing surfaces on DIII-D, both in the divertor and main chamber, are dominantly graphite tiles, and carbon is the dominant impurity in DIII-D during ELMing H-mode operation. The location of the primary source of the core carbon contamination has not been clearly identified. As a part of the effort to identify the primary sources of the carbon that reach the core plasma, methane puffing measurements have been carried out to supplement extensive spectroscopic measurements of neutral and molecular carbon [1].

The experiment was carried out in upper single null on DIII-D. A flux plot is shown in (Fig. 1). Methane was puffed from three locations: 1) from the outboard side between the midplane and the X-point, Fig 1 GASIW, 2) into the outer leg of the divertor from the private flux side, PFX1, and 3) from the inner wall, GASIW. To control the density in these ELMing

H-mode discharges,  $D_2$  was puffed from the outboard side (GASA) and was exhausted using the upper divertor cryopumps. Processed data will be shown from four discharges: 109296 and 109304, with the ion  $\nabla B$  drift direction up and line average densities of  $5 \times 10^{19} \text{ m}^{-3}$  and 109306, with  $\nabla B$  drift direction up and line average densities of  $8 \times 10^{19} \text{ m}^{-3}$ , and 110454 with the ion  $\nabla B$  drift direction down and a line average density of  $5 \times 10^{19} \text{ m}^{-3}$ . The GASD valve is fast acting with a nearly direct view of the vacuum vessel. The effective rise time of the puffed gas from this valve is a few milliseconds, and the shut off time is sub-millisecond. The PFX1 and GASIW valves are connected to their respective puffing zones by long capillary tubes, and have rise and fall times the order of 100 ms.

Selected time traces from shots 109296 and 109306 are shown in Fig. 2. In these shots the plasma current is ramped to a flat top of 1.3 MA at 1300 ms. From 1400 ms until the end of flat

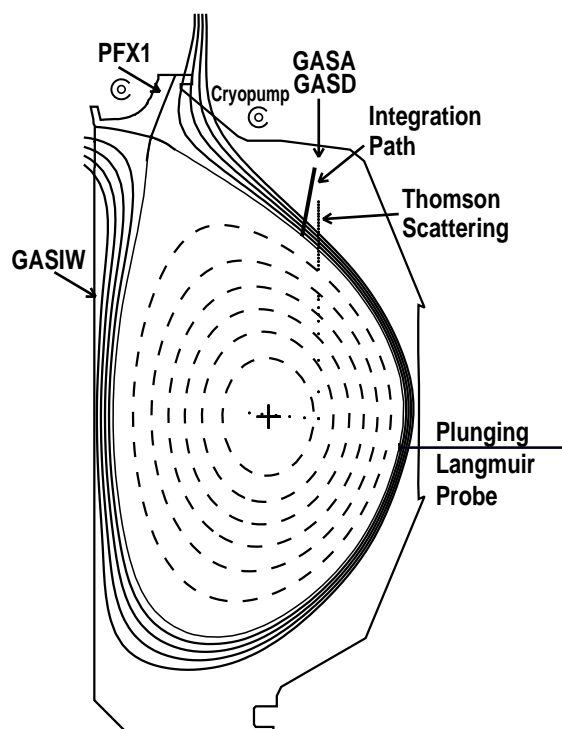


Fig. 1. A cross section of the DIII-D vacuum vessel is shown along with a flux plot from discharge 109296 at 3100 ms. The locations of the gas puffing valves used for the methane puffing experiments, of the Thomson scattering channels in the core and SOL plasma, and of the plunging Langmuir probe are also shown. GASA and GASD are at different toroidal locations. The line labeled as integration path in the upper outer SOL is the chord used in the 1-D attenuation model discussed in Section 3.

top at 5000 ms, injected beam power is fixed at 5.5 MW. The discharges transition into H-mode before 1800 ms. Type 1 ELMs begin shortly thereafter and continue throughout the flat top. Line averaged electron density [Fig. 2(a)] is increasing after the L-H transition, but in both discharges it reaches a stable level by 3000 ms. In discharge 109296, a stable operating density of  $5.6 \times 10^{19} \text{ m}^{-3}$  is maintained with no additional  $\text{D}_2$  gas puffing, but to maintain the higher density of  $8 \times 10^{19} \text{ m}^{-3}$  in 109306 a 190 Torr  $\ell/\text{s}$  puff is required [Fig. 2(b)]. In both discharges a methane ( $\text{CD}_4$ ) puff from GASD [Fig. 2(c)] is initiated at 2600 ms, and at 3350 ms, after the discharge has reached stable operation, the  $\text{CD}_4$  puff is turned off. The total  $\text{C}^{+6}$  content of the plasma [Fig. 2(e)], determined from charge exchange recombination spectroscopy (CER) [2,3], increases with the  $\text{CD}_4$  puff and then decays when the puff is turned off. After the carbon content has decayed from the GASD puff, a second  $\text{CD}_4$  puff from the PFX1 valve is initiated at 4100 ms [Fig. 2(d)] and continues until the end of flat top. The plasma stored energy [Fig. 2(f)] is reasonably constant, with an H<sub>ITER</sub>89P confinement scaling factor of 2.

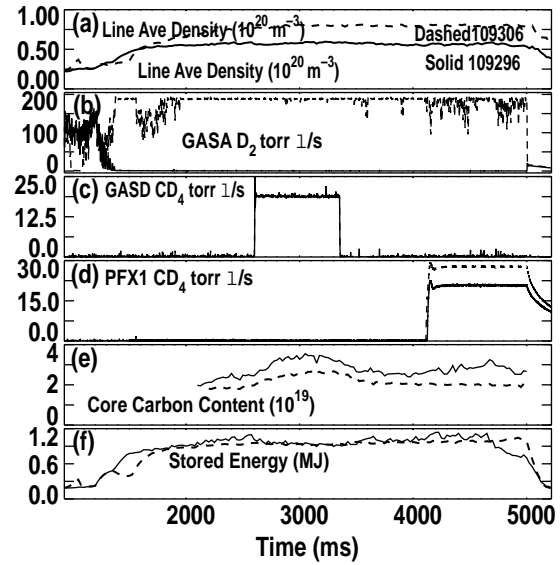


Fig. 2. Time traces of various measured plasma parameters are shown for discharges 109296 (black) and 109306 (red).

## 2. PENETRATION FACTOR

Here we define the penetration factor,  $P_f$ , as the ratio of the apparent source of carbon inside the separatrix (or in the core) to the throughput of methane from the gas valve. The throughput for each gas valve is calibrated off line and is accurate to  $\pm 5\%$ . Since the plasma has reached a steady condition by the end of the methane puff, the source of carbon in the core must equal the outflow of carbon from the core. The outflow is determined from the change in the total  $C^{+6}$  content of the plasma in the core due to the puff divided by the confinement time of  $C^{+6}$ . The total carbon content is obtained from the  $C^{+6}$  density profiles measured by the CER and integrated over the volume of the plasma using magnetic flux surface reconstruction from the EFIT code. The  $C^{+6}$  confinement time, the initial value of  $C^{+6}$  content and the background level of  $C^{+6}$  from the intrinsic sources are obtained from an exponential fit to the decay of the core  $C^{+6}$  content after the GASD methane puff is stopped. The time behavior of the core  $C^{+6}$  content for three discharges with GASD and PFX1 methane puffs is shown in Fig. 3 along with the exponential fits to the decay phase.

$$N^{C^{+6}}(t) = N_{\text{puff}}^{C^{+6}} e^{-(t-t_0)/\tau_C} + N^{\text{intr}} \quad , \quad (1)$$

where  $N_{\text{puff}}^{C^{+6}}$  is the core carbon content from the puff,  $\tau$  is the decay time, and  $N^{\text{intr}}$  is the offset due to intrinsic carbon. The core carbon source due to the puff is given simply by  $N_{\text{puff}}^{C^{+6}}/\tau_C$ .

Table 1 gives the results of the measured carbon confinement time, the energy confinement time and  $P_f$  for the three outer wall puff discharges considered here. Let's first compare the results of the density scan on the outer wall puff from the two discharges with ion  $\mathbf{B} \times \nabla \mathbf{B}$  drift direction toward the X-point, 109296 and 109306. We see that the increase in the line average density (Greenwald factor increase of 0.5 to 0.7) decreased the penetration factor by only 30%.

From table 1 we see that the inner wall puff had a larger  $P_f$  than the outer wall puff. Since the inner wall puffing valve has a relatively slow response time, the GASIW puff (discharge 109304)

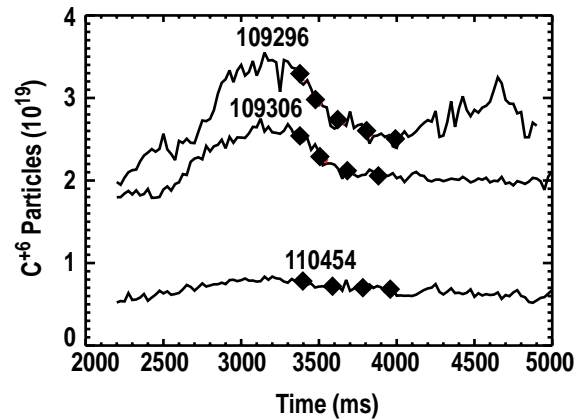


Fig. 3. The total core  $C^{+6}$  content is shown as a function of time for three discharges, 109296, 109306, and 110454 along with the exponential fits (diamonds) to the decay phase after the GASD valve is turned off. The time duration for the GASD and PFX1 valves is shown by the horizontal bars.

**Table 1. The parameters obtained from fitting the decay phase of the core carbon content and the calculated carbon penetration factor**

Discharge	Gas Valve	Puff Rate	$\tau$ (carbon)	$\tau_E$	$n_e$	$N_{\text{puff}}^{\text{C+6}}$	$N^{\text{INTR}}$	$P_f$
		$10^{20} \text{ s}^{-1}$	ms	ms	$10^{19} \text{ m}^{-3}$	$10^{19}$	$10^{19}$	%
109296	GASD	6.6	157	165	5.6	0.7	2.5	6.6
109304	GASIW	6.9	157*	176	5.0	1.1	3.8	10.1
109306	GASD	6.6	197	163	8.2	0.6	2.0	4.6
110454	GASD	6.5	167	168	5.0	0.12	0.7	1.1

\*taken from discharge 109296.

is held on sufficiently long that the gas throughput and the plasma response have both reached an equilibrium state. The change in carbon content due to the puff is taken as the increase in the total carbon content from the pre-puff level, and the carbon confinement time is assumed to be the same as measured in discharge 109296 following the GASD puff. The analysis of the divertor puff (PFX1) is problematic. In discharge 109296 there is an apparent increase in the carbon content due to the PFX1 puff. However in the other two discharges 109306 and 110454 (and in other discharges not shown here) the divertor puff had little or no apparent affect on the core carbon content. After 4000 ms in discharges 109296 (during the divertor region puff) and 109304 (during the inner wall puff) the plasma stored energy climbs slightly and the discharges show signs of encountering MHD instabilities. This MHD activity is more likely to be the cause of the increase in the carbon content at the end of discharge 109296 than the methane puff. Considering all the available data, we have determined that the divertor  $P_f$  is below the limit of measurability ( $< 1\%$ ). The increase in core carbon after 4000 ms in discharge 109296 is small compared to that in 109304 and introduces only a small error in the measurement of the inner wall penetration.

The most dramatic change in  $P_f$  occurs due to a change in toroidal field direction. When the ion  $\mathbf{B} \times \nabla \mathbf{B}$  drift direction is down (away from the X-point), the core carbon concentration is much lower both during and after the  $\text{CD}_4$  puff. As seen in Table 1 for discharge 110454, the  $P_f$  is also much lower, more than a factor of five below the comparable discharge with the ion  $\mathbf{B} \times \nabla \mathbf{B}$  drift direction up (109296).

### 3. SOL PROPERTIES AND NEUTRAL PENETRATION

The break up of methane and the resulting transport of carbon through the SOL is a complex process, but in the far SOL the electron temperature ( $< 10$  eV) is below or near the threshold for ionization and dissociation processes with ground state methane. The ion temperatures are high, the order of 100 eV, leading to fast charge exchange with deuterons [4]. At these low electron temperatures the dissociative recombination process with  $CD_4^+$  is fast, producing neutral radicals. This charge exchange/dissociative recombination process will likely cascade through the  $CD_y$  radicals, leading to the production of neutral carbon flux at about 1 eV temperature. In DIII-D a carbon neutral temperature of 1 eV is measured spectroscopically under conditions where chemical sputtering of hydrocarbon is expected to dominate over physical sputtering [1]. The neutral carbon that penetrates to the core from the methane puff is most likely due to the 1 eV carbon produced in the SOL from the stepwise dissociation of  $CD_4$ . SOL profiles of  $n_e$  and  $T_e$  for the low density and high density cases obtained from Thomson scattering and a plunging Langmuir probe are shown in Fig. 4. The results of a 1-D model for attenuation of an inward

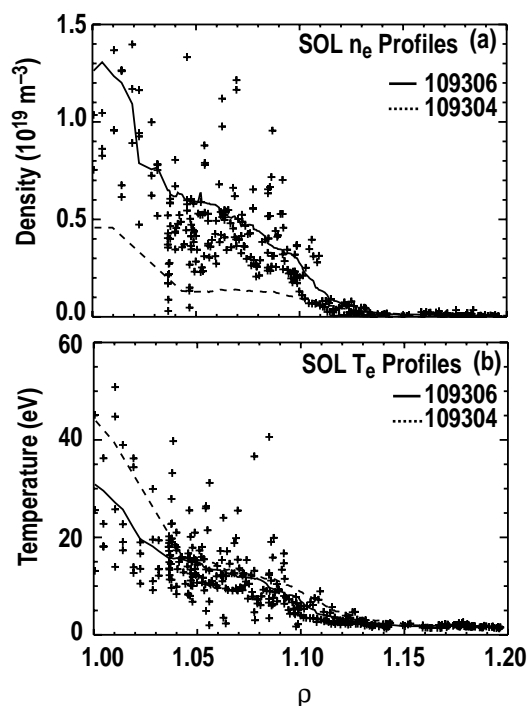


Fig. 4. The SOL profiles of electron density and temperature for 109304 and 109306 obtained from Thomson scattering and plunging probe measurements are shown. The curves are bin averaged over  $\Delta\rho = 0.03$ . The +'s are the original data for shot 109306.

flux of 1 eV neutral carbon originating at  $\rho = 1.2$  and using the SOL profiles shown in Fig. 4 are shown in Fig. 5, considering only electron impact ionization [5]. The charge exchange rate for deuterons onto neutral carbon is relatively weak [6]. The 1-D path chosen for the calculation shown in Fig. 5 goes through the SOL along a chord passing from the GASD valve through the magnetic axis of the plasma (see Fig. 1). For the lower line averaged density case, about 6.5% of the original carbon flux from the edge reaches the separatrix, in reasonable agreement with the measurement of 6.6% considering the crudeness of the model. However, in the higher line averaged density case the SOL electron density is almost three times higher while the SOL electron temperature remains about the same. The result is the calculated neutral carbon penetration is only about 0.26% while the measured value is 4.6%. The SOL electron density and temperature profiles for the  $\nabla B$  down case are not significantly different from the  $\nabla B$  up case at comparable line averaged density.

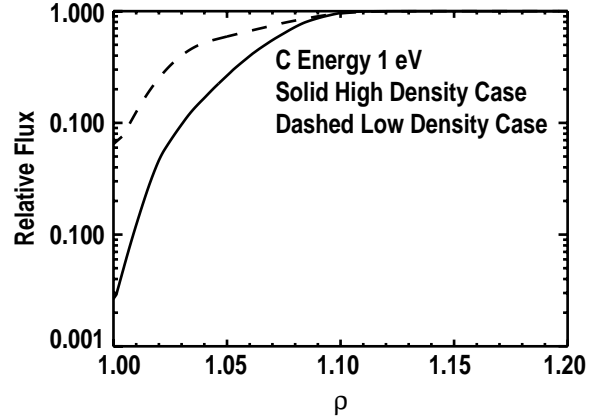


Fig. 5. The modeled attenuation of 1 eV neutral carbon as it penetrates the SOL along the chord shown in Fig. 1 for discharges 109304 and 109306. Only electron impact ionization is included in the model.

#### 4. MAIN CHAMBER CARBON SOURCE FROM CHEMICAL SPUTTERING

We can use the measured penetration factors to get a rough estimate of the core contamination due to chemical sputtering at the main chamber wall. An estimate of the wall flux of methane into the SOL plasma at the midplane can be obtained from a spectroscopic measurement of the intensity of the CD emission band at 4305 Å. After correcting for geometric factors, the band intensity can be converted to the methane flux,  $\Gamma_{\text{CD}_4}$ , using the measured photon production efficiencies of 100 CD<sub>4</sub> molecules/photon at typical SOL electron temperatures [7,8]. Assuming poloidal uniformity, the core carbon content,  $N_C$ , is then given by

$$N_C = \Gamma_{\text{CD}_4} \times P_f \times A_{\text{sep}} \times \tau_C \quad (2)$$

where  $A_{\text{sep}}$  is the surface area of the last closed flux surface. The fraction of core carbon is given by  $N_C/N_e$ , where  $N_e$  is the total electron content of the plasma. In discharge 109296, the low density case, the SOL emissivity of the CD band is measured to be  $2 \times 10^{18}$  ph/cm<sup>2</sup>/s resulting in a methane influx of about  $1 \times 10^{20}$  m<sup>-2</sup>. From Eq. (2) we obtain a core carbon fraction of 1% to 5%. A range is quoted due to uncertainty in the geometric corrections and poloidal uniformity. Using CER data, the measured core carbon fraction is found to be 3%, indicating that main chamber chemical sputtering is playing a significant role in core contamination.

## 5. DISCUSSION

In the limited density scan reported here the penetration of carbon into the core plasma decreases only slightly as the line averaged density was increased from  $5 \times 10^{19} \text{ m}^{-3}$  to  $8 \times 10^{19} \text{ m}^{-3}$  even though the SOL density and opacity to neutral C increased much more. The ansatz of SOL shielding by neutral ionization seems to be too simple. The carbon content in the core plasma is controlled not only by the carbon source inside the separatrix, but also by the carbon density at the separatrix, i.e. the boundary condition presented by the wall source and the SOL impurity transport. The SOL transport of carbon ions, which sets the carbon density boundary condition for the core, may be more important in determining the core carbon content than the penetration of neutrals. Changing the direction of the toroidal magnetic field, which changes both the  $\mathbf{B} \times \nabla \mathbf{B}$  and  $\mathbf{E} \times \mathbf{B}$  drift directions, made a very large change in the core carbon content due to both intrinsic and puffed sources of carbon. This fact suggests that drifts are important in SOL impurity transport. The fact that drifts play an important role in SOL impurity transport has been shown previously [9]. Achieving a detailed predictive capability of core impurity contamination will require the coupling of edge plasma transport models that include drift terms to core transport models. The penetrations factors, combined with a spectroscopic measurement of the SOL CD emission, indicate that main chamber chemical sputtering is an important contributor to carbon contamination of the core plasma.

**REFERENCES**

- [1] R.C. Isler, R.J. Colchin, N.H. Brooks, T.E. Evans, W.P. West, D.G. Whyte, *Phys. Plasmas* **8** (2001) 4470.
- [2] K.H. Burrell, D.H. Kaplan, P. Gohil, D.G. Nilson, R.J. Groebner, and D.M. Thomas, *Rev. Sci. Instrum.* **72**, (2001) 1028.
- [3] M.R. Wade, W.A. Houlberg, L. R. Baylor, *Phys. Rev. Lett.* **84**, (2000) 282.
- [4] R.K. Janev and D. Reiter, Report FZJul. (2002) 3966.
- [5] H.P. Summers, ADAS, Atomic Data and Analysis Structure, Originally developed by the Jet Joint Undertaking, 1st Addition User Manual, (1994).
- [6] P.C. Stancil, J-P Gu, C.C. Havener, P.S. Kestic, D.R. Schults, et al., *J. Phys. B: At. Mol. Opt. Phys.* **31**, (1998) 3647.
- [7] M.F. Stamp, S.K. Erents, W. Fundamenski, G.F. Matthews, R.D. Monk, *J. Nucl. Mater.* **290-292** (2001) 321.
- [8] D. Naujoks, D. Coster, H. Kastelewicz, R. Schneider, *J. Nucl. Mater.* **266-269** (1999) 360.
- [9] S. Gangadhara, B. LaBombard, C. MacLatchy, *J. Nucl. Mater.* **290-293** (2001) 598.

## **ACKNOWLEDGMENT**

Work supported by U.S. Department of Energy under Contracts DE-AC03-99ER54463, W-7405-ENG-48, DE-AC05-00OR22725, DE-AC02-76CH03073, and Grant DE-FG03-95ER54294.